UC Berkeley
UC Berkeley Previously Published Works

Title
Measurement of colloidal phenomena during flow through refractive index matched porous media

Permalink
https://escholarship.org/uc/item/9059408z

Journal
Review of Scientific Instruments, 86(11)

ISSN
0034-6748

Authors
Roth, Eric J
Mont-Eton, Michael E
Gilbert, Benjamin
et al.

Publication Date
2015-11-01

DOI
10.1063/1.4935576

Peer reviewed

Measurement of colloidal phenomena during flow through refractive index matched porous media

Eric J. Roth[1], Michael E. Mont-Eton[1, a)], Benjamin Gilbert[2], Tim C. Lei[3], *and* David C. Mays[1, b)]

- [1]Department of Civil Engineering, University of Colorado Denver, Campus Box 113, P.O. Box 173364, Denver, Colorado 80217-3364, USA

- [2]Earth Sciences Division, Lawrence Berkeley National Laboratory, Mail Stop 74R316C, 1 Cyclotron Road, Berkeley, California 94720, USA

- [3]Department of Electrical Engineering, University of Colorado Denver, Campus Box 110, P.O. Box 173364, Denver, Colorado 80217-3364, USA

- [a)]Now at Buckley Air Force Base, 18500 East Sixth Avenue, Aurora, Colorado 80011, USA.

- [b)]Author to whom correspondence should be addressed. Electronic mail: david.mays@ucdenver.edu. Telephone: 303-352-3933.

ABSTRACT

Colloidal phenomena in porous media, natural or engineered, are important in a breadth of science and technology applications, but fundamental understanding is hampered by the difficulty in measuring colloid deposit morphology *in situ*. To partially address this need, this paper describes a static light scattering apparatus using a flow cell filled with refractive index matched (RIM) porous media, allowing real-time measurement of colloidal phenomena as a function of depth within the flow cell. A laser interacts with the colloids in the pore space and their structures, but not with the RIM media. The intensity of scattered light is measured as a function of scattering angle, which allows characterization of colloid deposit morphology as a fractal dimension and a radius of gyration. In parallel, fluid discharge rate and pressure drop are recorded to determine permeability, a key parameter for any application involving flow through porous media. This apparatus should prove useful in any application requiring characterization of colloidal phenomena within porous media. Additionally, this paper describes how to use granular Nafion as RIM porous media.

I. INTRODUCTION

Flow through porous media is common to numerous engineered and natural systems such as granular media reactors, filters, soils, groundwater aquifers, and petroleum reservoirs. In each of these applications, colloids—particles with characteristic sizes ranging from 1 nm to 10 μm—exert major influences on solute transport, reaction catalysis, and the permeability of the porous media itself. It is widely recognized that colloidal phenomena in porous media are very complex and more information is needed at the pore scale.[1–7]

Currently, there are a number of imaging techniques available for characterization of colloidal phenomena in saturated porous media. Optical imaging techniques often employ visible and fluorescent light in conjunction with high resolution digital cameras to achieve a resolution of 0.15×0.15 mm^2.[8] This can be a useful method for tracking colloid migration, but common colloids, like montmorillonite clay, are discs with a diameter of 1 $μm$ and a thickness of only 1 nm,[9] with aggregate structures of $0.1 - 2$ $μm$ characteristic size.[10] Unfortunately, optical imaging resolution is not fine enough to resolve colloid aggregates at these scales. Optical imaging can go further by employing fluorescent microscopy to evaluate pore scale processes at a resolution of 0.7×0.7 $μm^2$,[8] but this is a difficult technique, requiring continuous calibration and image correction due to the non-uniformity of light sources. Using fluorescent microscopy, the resolution gets closer to the scale of the colloid aggregates, but the length of time required to take successive images can be problematic due to the transient nature of colloidal phenomena during flow. Pore space tomography measures pore structure at still finer resolution, but not yet sufficient to resolve colloidal phenomena. Specifically, the resolution limit is 100 μm for thermal neutrons,[11] 10 μm for magnetic resonance imaging,[12] and 2 μm for synchrotron x-ray computed microtomography.[5,13]

Because direct imaging techniques are currently unable to directly determine the structure of colloidal deposits, we sought to provide structural characterization through static light scattering (SLS). In particular, several authors have suggested that the deposits that cause clogging may exhibit a fractal aggregate morphology,[4,14] as seen for flocculated particles in bulk fluids.[15] This paper reports a novel experimental apparatus designed to measure colloid deposit morphology as a fractaldimension and a radius of gyration, using SLS in a flow cell filled with refractive index matched (RIM) porous media. SLS is a standard technique[16–20] for measuring fractal dimension and radius of gyration. The feasibility of measuring colloid aggregate fractal dimension in RIM porous media has been demonstrated previously.[21] The contributions of this work, therefore, are (1) to extend SLS to a flow cell filled with RIM porous media, (2) to record SLS data as a function of vertical position, (3) to report results not only for fractal dimension but also for radius of gyration, and (4) to quantify goodness-of-fit for the fitted fractal dimensions and radii of gyration. We also provide detailed evaluation of the use of Nafion as RIM in solutions of varying ionic strengths. It is crucial that the experimental setup for this research includes a high resolution (less than 100 nm), non-destructive technique with real time measurement of colloid deposition (i.e., accumulation) and colloid deposit morphology. Achieving these goals using SLS requires that measurements be performed in a flow cell containing RIM (i.e., transparent) porous media.

The idea of fractal dimension was popularized by Mandelbrot in 1967.[22] Briefly, fractal dimension is a measure of geometric complexity as a function of scale, which makes it useful in describing the compactness of a shape (Figure 1). Accordingly, fractal dimension is a standard approach for describing aggregate structures.[17,23] For the present study, the fractal dimension is taken to be a mass fractal dimension, which is defined by the mass length relationship

$$M \propto L^{D}, \tag{1}$$

where M is the aggregate mass, L is the characteristic length, and D is the fractal dimension. Aggregate mass can be recalculated as N, the number of colloids,

$$N = k\left(\frac{R_g}{r}\right)^{D}, \tag{2}$$

where k is a constant of proportionality, R_g is the radius of gyration, r is the colloid radius, and D is the fractal dimension.

FIG. 1. Conceptual illustration of colloid deposits with primary particles of diameter 105 nm, radius of gyration 707 nm, and fractal dimensions of (a) 1.3, (b) 1.6, (c) 1.9, and (d) 2.2. Figures generated using DLA version 1.13.02.[44]

PPT
High-resolution

The experimental apparatus described in this paper includes a number of other important features, including (1) an improved flow cell-manifold interface and quick mounting system for the manifold to the SLS bench, (2) a light proof, dust inhibiting, cooling system with vibration isolation, (3) a vertical actuator for the flow cell, and (4) pressure transducers, from which permeability can be calculated from the known apparatus geometry, flow rates, and fluid properties. Due to the nature of the experiment, it is also necessary that SLS scans are made quickly, and that the SLS apparatus can be easily modified to accommodate both flow-through and batch samples. The apparatus also supports the development of several novel experimental methods, including a method for measuring specific deposit with the SLS apparatus and a method for measuring the porosity of RIM porous media.

II. METHODS

An overview of the apparatus and its operation is given in Figure 2. Briefly, a colloid suspension is eluted through a glass column packed with RIM porous media. Laser light scatters from the colloids and their structures, but not—ideally—from the transparent porous media. The intensity of scattered light, I, is measured over a range of scattering angles, θ, which allows determination of the fractal dimension and the radius of gyration as described below. The flow cell is mounted on a vertical stage, which allows repeated measurements from the top to the bottom of the flow cell. Discharge, defined as fluid volume passing through the flow cell per unit time, and pressure drop are recorded independently to determine permeability. These steps are elaborated in Secs. II A–II E on apparatus design, porous media, colloid suspension, experimental procedures, and data reduction.
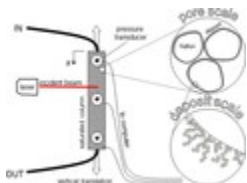

FIG. 2. Experimental schematic.

A. Apparatus design

The optical-quality glass flow cell (Adams and Chittenden Scientific Glass, Berkeley, California) has an outer diameter of 15 mm, an inner diameter of 12 mm, and a length of 100 mm (Figure 3). The cell has four pressure ports and is positioned between custom-fabricated upper and lower manifolds fitted with rubber O-rings and custom seats to make a watertight seal. The assembly is then mounted on a vertical stage (Zaber Technologies, TLSR150A, Vancouver, Canada) allowing SLS measurements to be recorded at any point along the length of the flow cell.

FIG. 3. Flow cell detail.

Flow is provided by a peristaltic pump (Cole Parmer, Masterflex L/S, Vernon Hills, Illinois) with precisely calibrated parallel heads, one drawing from a reservoir containing stable colloids (i.e., colloids in salt-free water) and the other drawing from a reservoir containing a salt solution. The two sources join at a confluence point just upstream of the entry point to the flow cell and then proceed through the porous media. Separation of these two sources is necessary, in our particular application, to postpone colloid aggregation until the fluid has entered the flow cell. Separation would not be required in other applications where such postponement was not a concern. The flow rate coefficient of variation has a range of 0.1%–2.0% depending on the experiment. Fluid exits the flow cell to waste.

Pressure drop is measured across the pressure ports on the flow cell (Figure 3). Tubing from each port is routed into one of the four differential pressure transducers (Validyne, DP15, Northridge, California) that provide data logging with vendor-supplied software. Pressure drop is measured over four distinct regions: inlet, middle, and outlet regions of the flow cell, and one overall pressure drop measurement from the top to bottom of the flow cell manifold (Figure 3). Transducer diaphragms are selected based on expected pressure measurements, with the goal of selecting the most sensitive diaphragm that will also be rugged enough to avoid damage due to exceeding the maximum suggested pressure. The chosen diaphragms have standard errors of 0.25% of full scale, with full scales of 14, 35, or 140 cm H_2O. Transducers are calibrated by manometer before each experiment. Prior to experimental measurement, care is taken to eliminate any air in the system.

Laser light is generated by an intensity-controlled helium-neon laser with a wavelength of 633 nm (Spectra-Physics, 117A, Santa Clara, California). The laser beam first passes through a half-wave plate followed by an optical polarizer for intensity adjustment (Figure 4). The optical polarizer also ensures that the polarization (direction of the electric field) of the laser beam is perpendicular to the optical table (s-polarized to the flow cell). An optical chopper (Stanford Research Systems, SR540, Sunnyvale, California) is also placed in the beam path for lock-in detection. Because the entering and exiting surfaces of the flow cell are curved, they act as focusing elements to the laser beam in the horizontal direction. To compensate for this focusing effect, a

cylindrical lens (f = 25 mm, Thorlabs, Newton, New Jersey) is placed in front of the flow cell. After the laser beam passes through the flow cell, it is captured by a beam-block to prevent it from getting into the detector assembly.
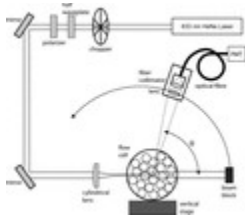

FIG. 4. Static light scattering (SLS) components. PMT means photomultiplier tube. Not to scale.

PPT
High-resolution

The detector assembly is constructed with a lens, a fiber collimator, and a single-mode optical fiber,which are all mounted on a rotational stage (Newport, URM80ACCHL, Irvine, California) that allows for angular scanning around the flow cell. The lens to collect scattered light (1 inch diameter and f = 500 mm, Thorlabs, Newton, New Jersey) is positioned 180 mm away from the flow cell axis and 40 mm away from the optical fiber, rendering a magnification of (180 mm)/(40 mm) = 4.5. The lateral focal diameter of the lens at the flow cell center is calculated to be approximately 100 μm based on the Gaussian beam equation. An optical collimator (F260FC-B-633, Thorlabs, Newton, New Jersey) is then connected to a single-mode optical fiber (P1-630A-FC-1, Thorlabs, Newton, New Jersey), and then positioned behind the lens in order to focus the collected scattered light into the single-mode optical fiber. The optical fiber has a core diameter of 4.3 μm, which acts as a pinhole to prevent out-of-focus light along the axial direction from entering the optical fiber. With the magnification of 4.5, the effective sample width perpendicular to the line connecting the flow cell axis to the detector assembly, from which scattered light is collected, is approximately 4.5 (4.3 μm) = 19 μm. The optical fiber has a numerical aperture of 0.14 which, with the collimating and the front lenses, translates to an angular resolution for the entire detector assembly of approximately 0.25°. The numerical aperture also renders a sample width parallel to the line connecting the flow cell axis to the detector assembly of (3.5/0.14) (19 μm) = 480 μm. The distal end of the optical fiber is connected to a photomultiplier tube operating in the linear mode to amplify the incoming optical signal (Hamamatsu, H9858-20, Hamamatsu, Japan), which is mounted to the optical table in a secured position. Finally, the detected signal is analyzed by a lock-in amplifier (Stanford Research Systems, SR830, Sunnyvale, California) allowing for improved signal sensitivity and noise rejection. A custom program written in LabVIEW (National Instruments, Austin, Texas) is used to control the entire system.

The intensity of light scattered from colloids within the RIM porous media as a function of scattering angle is measured by the rotating detector assembly (Figure 4), where the LabVIEW program sets the rotational stage at 160 logarithmically spaced angles between 0.43° and 151.66° for approximately 0.5 s each, such that the time required to record a single angular scan is approximately 90 s. Moving the flow cell vertically, also controlled by the LabVIEW program, required approximately 30 s per move, such that recording angular scans at each of three elevations requires approximately 360 s. The entire apparatus is constructed on a vibration-isolated optical bench enclosed by a light shroud. Previously reported experiments, in which batch samples were placed in optical cuvettes rather than the flow cell reported here, indicate that background scattering from the RIM porous media is at least one order of magnitude less than the scattering from the porous media with colloids and confirm proper alignment matching theoretical Mie scattering for 1 μm colloids (see Figure 4 of Mays *et al.*[21]). More elaborate details on the SLS measurement process are available in Mont-Eton[24] and Roth.[25]

B. Porous media

SLS requires the porous media to be RIM with the saturating fluid, that is, essentially transparent. Candidate pairs of porous media and fluids, with matching index of refraction n, may be selected from tables reported in the literature.[26-28] In our particular application, Nafion (C.G. Processing, Rockland, Delaware), a synthetic ionomer, was found to be a suitable RIM porous medium for a number of reasons. First, index matching is possible with an inexpensive azeotrope of isopropanol and water whose environmental, safety, and health considerations are easily manageable. Second, Nafion grains retain enough colloids to make practical measurements of colloidal phenomena within porous media. Third, hydrated Nafion has a sufficiently rigid structure as to minimize deformation during fluid flow, which allows a preliminary SLS scan to be used as a colloid free blank which, as described below, is subtracted from the measured light intensity during data reduction. And fourth, using Nafion allows control of colloidal stability through modification of the salt concentration,[29] which is crucial in our particular application.

In order to limit porous media realignment during experiments, enough Nafion is added to the flow cell to place it under slight compression after hydration-induced-swelling. An azeotrope of 42% isopropanol and 58% deionized water by volume provides refractive index matching with Nafion[21] and is therefore used as the suspension fluid in the experiments reported here. The fluid is vacuum-filtered three times through a 0.2 µm filter (Whatman, Polyamide NL-16, Dassel, Germany) prior to Nafion hydration. At 20 °C, the data reported by Pang et al.[30] were interpolated to estimate this azeotrope's density as 958 kg/m^3 and dynamic viscosity of 3.0 × 10^{-3} kg m^{-1} s^{-1}. Working with Nafion requires particular attention to detail, as elaborated in the following paragraphs.

The Nafion used here was granular with diameters ranging from 0.50 to 1.18 mm (i.e., passing a standard #16 mesh but retained on a standard #35 mesh). This size range is much larger than the largest length scale probed by our SLS apparatus, which is approximately Q_{min}^{-1}; so with $Q_{min} \approx 10^{-3}$nm^{-1}, this length scale is approximately 1 µm. Accordingly, there is no influence by the structure of the porous media on the measured scattering, providing the refractive index is matched to the fluid. Within the granular Nafion size range of 0.5-1.18 mm, the distribution of grain size changes from batch to batch, and due to vibration during handling, smaller grains settle to the bottom of containers. Therefore, in order to have reproducible porous media between experiments, it is necessary to combine and thoroughly mix different batches of Nafion. To keep Nafion evenly mixed in the container, the container should be repeatedly inverted before apportioning. In order to achieve saturated conditions, it was found that hydrating dry Nafion inside the flow cell was the most efficient way to load the Nafion and purge air from the pore space. Formation of bubbles was minimized by saturating the Nafion from the bottom up, flushing overnight, and maintaining positive gage pressure. When bubbles appeared, results were discarded and experiments repeated. Nafion grains approximately double in size upon hydration. The result is that small dry grains can swell inside flow cell orifices (i.e., inlets, outlets, and pressure ports), causing the orifices to become obstructed. To minimize this problem, inlets and outlets are fitted with screens, and pressure ports are fitted with short lengths of 1 mm tubing passing through the port and into the Nafion. Early experimentation indicated that altering the flow velocity led to changes in Nafion's permeability, which took a significant time to regain equilibrium. Accordingly, constant flow rates are used. Even during Nafion hydration, the flow rate should match to that of the experiment.

Though Nafion can accommodate saline solutions, ionic strength has a dramatic effect on Nafion swelling, with significantly reduced swelling at higher salt concentrations (Table I). Consequently, higher salt concentrations lead to higher porosity; although when using magnesium chloride for the salt, this effect is less pronounced at ionic strengths above 5 mM. At lower salt concentrations, the Nafion is extremely sensitive. Variations of salt content as low as ±0.1% produce changes in Nafion permeability. Temperature also affects the swelling potential of Nafion, although to a smaller extent than ionic strength. Care should be taken to ensure stable

temperatures during experiments. As with other physical and chemical conditions of the experiment, Nafion requires ample time to adjust to changes before making any measurements.

TABLE I. Porosity at various salt concentrations.

MgCl$_2$ concentration (mM)	Ionic strength (mM)	Porosity
1	3	0.05
2	6	0.11
4	12	0.22
8	24	0.26
16	48	0.26

Porosity is determined by measuring the volume of vegetable oil (Kroger Company, Cincinnati, Ohio) required to displace the azeotrope between swollen Nafion grains previously in equilibrium with the azeotrope at a known salt concentration. Oil is injected into the top of the flow cell in order to displace the higher density isopropanol-water azeotrope downward, and porosity is calculated by dividing the volume of oil by the total flow cell volume, with an estimated standard error of ±0.01. Because Nafion swelling is sensitive to salt concentration, porosity is measured separately for each salt concentration used. In preliminary experiments, dry and swollen Nafion was saturated in vegetable oil for several days, which provided no evidence that vegetable oil had any effect on Nafion.

C. Colloid suspension

The colloids used are carboxylate-modified polystyrene microspheres (Seradyn, Indianapolis, Indiana) with a uniform diameter of 106 nm and a refractive index of 1.55-1.59.[24] When dispersed in the isopropanol-water mixture, these colloids remained stable and showed no evidence of swelling (see Figure 4(c) of Mays *et al.*[21]). Colloid stability—the ability to resist aggregation or deposition—is adjusted by varying the salt concentration in accordance with classical Derjaguin-Landau-Verwey-Overbeek (DLVO) theory.[29] The salt selected here is magnesium chloride (Fisher Scientific, Fair Lawn, New Jersey). In our particular application, a key parameter is the critical coagulation concentration (of salt) above which the colloids will aggregate. To find the critical coagulation concentration, varying amounts of salt are added to the isopropanol-water azeotrope with a colloid concentration of 100 ppm. For the colloids used in the experiments, a salt concentration between 1 and 1.1 mM of MgCl$_2$ will lead to aggregate settling within 24 h.

D. Experimental procedures

Solutions are prepared and glassware is thoroughly washed in a caustic detergent, and then rinsed with deionized water in advance of performing experiments. The appropriate amount of dry Nafion is added to the flow cell and then hydrated with the isopropanol-water azeotrope. The Nafion is allowed to equilibrate

overnight with a constant flow of fresh azeotrope. The next day, the flow cell is connected to pre-calibrated transducers. Colloid-free flow is initiated at the target flow rate, data logging is initiated, and equilibrium is confirmed when the permeability becomes stable, which indicates that the Nafion is no longer swelling or compressing. Next, the incident laser beam alignment with the flow cell is confirmed. A blank scan of the flow cell with RIM porous mediawithout colloids is recorded, to be used in later calculations. Deposition flow (i.e., flow with colloids) is then started. At various times during each experiment, scans are performed at three different vertical positions: near the inlet, the middle, and near the outlet. The first time is during deposition flow; the second time is after flow is stopped; and the third time is after clear flow (i.e., flow without colloids) is started, which flushes any suspended colloids or aggregates from the pore space and therefore isolates scattering from colloid deposits.

E. Data reduction

Colloid aggregate morphology, specifically fractal dimension, and radius of gyration, are determined from the relationship between normalized, background-subtracted scattering intensity and the scattering wave vector. Specifically, the intensity of scattered light, I, is normalized to $I' = I/(\tau A)$, where τ is the transmission factor, and A is proportional to the scattering area.[21] The transmission factor τ is the ratio of transmitted intensity measured at $\theta = 0°$ to the incident intensity, and $A \sim 1/\sin(\theta)$. Because there is inevitably some light scattering from the nominally transparent porous media, the normalized intensity is background-subtracted, which defines $I'' = I'_{sample} - I'_{blank}$. Scattering from the blank is typically at least one order of magnitude less than scattering from the sample, such that colloid scattering dominates the normalized intensity over the full range of Q. At low angles, it is necessary to protect the photodetector from the incident laser beam at $\theta = 0$, whose intensity is orders of magnitude larger than the scattered light. Accordingly, the minimum scattering angle at which data were recorded was $\theta = 0.43°$. At low angles, the scattering intensity is generally high enough to saturate the photodetector, in which case data are omitted, such that the minimum angle used is the smallest angle at which the photodetector is not saturated. At large angles, it is observed that scattering intensity begins to increase for $\theta > 90°$, which is attributed to diffuse reflection of the incident beam from surface of the glass flow cell. Accordingly, intensity data are disregarded when either the sample or the blank shows saturation, or when $\theta > 90°$.

The scattering angle θ is converted to the scattering wave vector,[17]

$$Q = \frac{4\pi n}{\lambda} \sin\left(\frac{\theta}{2}\right),$$

(3)

where n is the index of refraction of the fluid and λ is the wavelength of the laser. These reduced data are then analyzed on a plot of $\log(I'')$ versus $\log(Q)$, an idealization of which is shown in Figure 5. According to the standard interpretation of these SLS data,[20] this plot has three general regions. At small $Q < 1/R_g$, I'' is approximately constant, reflecting a lack of structure at scales larger than the aggregate (or deposit) scale. At large $Q > 1/r$, I'' displays Mie humps that result from light interference around individual colloids. At intermediate Q, $1/R_g < Q < 1/r$, the slope of $\log(I'')$ versus $\log(Q)$ is approximately linear with a downward slope equal to the fractal dimension D. This linear region is the basis for a simple, two-parameter model[20] used to determine the fractal dimension and a scaling factor with arbitrary units (a.u.). Standard errors for this two-parameter model are determined during linear regression.[31] A more sophisticated, three-parameter model[32] determines both fractal dimension and radius of gyration, using the entire data set, not just the linear region. Standard errors for this three-parameter model are estimated using the bootstrap.[33] Briefly, the bootstrap estimates standard errors by first creating B bootstrap replicates, each of which contains n pairs if (Q, I'') randomly selected with replacement from the n pairs of (Q, I'') in the measured data. The three

parameters are fitted to each of the B bootstrap replicates, and the resulting distributions of each estimated parameter are used to estimate standard errors. The number of replicates chosen is $B = 100$, after which the distributions of the estimated fractal dimension D, the estimated radius of gyration R_g, and the estimated scaling factor k were shown to stabilize during preliminary numerical experiments (not shown). The Akaike information criterion (AIC)[34] is used to assess which model should be used. When the two parameter model fits the data better, it is deemed that no radius of gyration information is available.
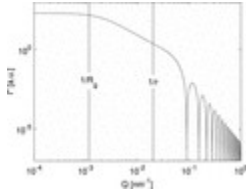
FIG. 5. Theoretical IQ plot for determination of fractal dimension, D, and radius of gyration, R_g, plotted using $I'' = kPS$, where the scaling factor k is arbitrary, the form factor P is given by Equation (55) in Pedersen,[45] and the structure factor S is given by Equation (16) in Teixeira.[32]

PPT
High-resolution

The amount of colloid accumulation within porous media is quantified using the specific deposit, σ, defined as the volume of deposited colloids per total volume of the flow cell. In order to determine specific deposit independently of deposit morphology, a calibration curve containing normalized and background-subtracted scattering intensity, I'', versus pore fluid concentration, C_{pore}, is used (Figure 6). The calibration curve is constructed from known pore fluid concentrations and intensity measurements at the angle where the scattering wave vector $Q = 1/r$, where one can assume that scattering is independent of deposit morphology, because the structure factor $S(Q)$ becomes constant for $Q > 1/r$.[20] Numerical calculations (not shown) based on the theoretical IQ curve in Figure 5 have confirmed this assumption to be reasonable. The resulting measurement of C_{pore} is relevant to the precise area of the flow cell scanned. In constructing the calibration curve, it was observed that I'' for $C_{pore} < 10$ ppm were indistinguishable from background noise. At higher concentrations, above 300 ppm, error became significant, such that the root mean squared error (RMSE), averaged over the entire calibration curve, is 34%. The specific deposit is then calculated by $\sigma = nC_{pore}$.
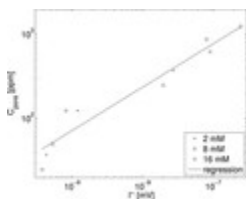

FIG. 6. Calibration curve used to determine pore fluid concentration, C_{pore}, as a function of the normalized, background-subtracted scattering intensity, I'', measured at $Q = 1/r$. The regression equation is $C_{pore} = 3.12 \times 10^6 (I'')^{0.515}$ ($R^2 = 0.93$).

PPT
High-resolution

III. RESULTS

Typical $\log(I'')$ versus $\log(Q)$ results are shown in Figure 7. In this particular experiment, the salt concentration of 2 mM of $MgCl_2$ exceeds the critical coagulation concentration. The porosity is 0.11 ± 0.01 (as shown in Table I), the discharge is 15.8 ± 0.3 mL/min, the specific discharge is 201 ± 4 m/d, and the average fluid velocity

is 1825 ± 169 m/d. This particular scan is recorded at the midpoint of the flow cell during a period of no flow, after eluting 274 ± 25 pore volumes of fluid with an influent concentration of 125 ppm. At this point, the pore fluid concentration, determined from the calibration curve using scattering data at $Q = 1/r$, is 1077 ± 366 ppm, corresponding to a specific deposit of 118 ± 42 ppm, which reduced the permeability to 66 ± 0.1% of its initial value. For this scan, the AIC for the two-parameter model is −442, while for the three-parameter model, it is −561, so accordingly the three-parameter model is used to determine the fractal dimension $D = 1.69 ± 0.07$ and the radius of gyration $R_g = 673 ± 50$ nm. The superior fit of the three-parameter model versus the two-parameter model is also apparent from visual inspection of Figure 7. Additional measurements from the apparatus reported here are reported in a separate study linking permeability to colloid deposition under a range of hydrodynamic and chemical conditions.[35]
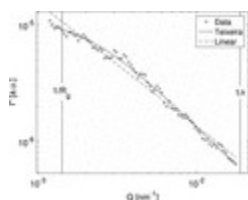

FIG. 7. Typical results showing SLS measurements (+), the two-parameter model (dashed line), and the three-parameter model of Teixeira[32] (solid line). A conceptual illustration of the colloid deposit generating these results is provided in Figure 1(b).

PPT
High-resolution

IV. DISCUSSION

The apparatus described here offers a number of distinct advantages over previously published instruments for characterizing colloidal phenomena within porous media. First, measurements from our SLS apparatus proved repeatable and consistent with the applicable scattering theory as indicated by small RMSE. Second, measurements of fractal dimension are precise, with typical errors (i.e., root mean squared errors estimated by the bootstrap) less than ±0.05. Third, the speed at which SLS scans are completed is also noteworthy. Once the SLS scans are ready to commence, each scan only takes approximately 90 s. And fourth, the SLS apparatus is adaptable: able to handle the alterations required to make measurements in either batch or flow mode, to accommodate the plumbing required to operate pressure transducers, and to handle the challenges that come with the sensitive nature of RIM granular Nafion. The key to this adaptability comes mostly by way of economizing space. The usable space on the bench measures roughly 1.5 m wide by 0.6 m deep by 0.8 m high, leaving enough room to add components while also helping to mitigate thermal hot spots created by system components. The apparatus could be scaled up for different experiments with the addition of a larger bench and a larger light shroud.

As an added benefit, the adaptability of the apparatus could lend itself to a multitude of different applications for various fields of study where characterization of colloidal phenomena is necessary within porous media. Applications include characterization of colloid deposits to correlate with permeability of natural or engineered porous media,[4] observation of coupled aggregation and sedimentation as a function of depth,[36] measurement of the fractal-to-crystal transition during protein aggregation,[23] and determination of the scattering structure factor of colloidal gels.[37]

Because of multiple scattering, use of SLS to study deposition processes requires care in data interpretation when the transmission factor, τ, is less than approximately 80%. There is agreement that multiple scattering does not affect the determination of radius of gyration from SLS measurements,[18,38] but less consensus on whether multiple scattering affects the determination of fractal dimension. We previously investigated multiple

scattering effects using the same microspheres and SLS system described here, finding no dependence of fractal dimension upon concentration between 5 and 80 ppm with transmission factors 43% ≤ τ ≤ 85%.[21] Other experimental studies also reported negligible effect of multiple scattering on the determination of fractal dimension.[39–41] In contrast, recent numerical simulations by Yon *et al.*[38] found that multiple scattering could lead to inaccurate measurement of fractal dimension for combustion generated soot aggregates. The concerns they raise are not applicable here, however, because scattered light is collected by a single-mode fiber whose effective sample width, the larger of the perpendicular width of 19 μm and the parallel width of 480 μm, is smaller than the mean free path of scattering for the colloids used. Specifically, using the average colloid index of refraction $n = 1.57$ and our maximum colloid volume concentration of 2.14×10^{-3} nm^{-1}, the corresponding minimum mean free path of scattering is 1500 μm, determined with Equation (28) in Wiese and Horn[42] and Equation (34) in Sorensen.[20] Accordingly, for the apparatus and colloids described here, significant multiple scattering contributions are avoided. More generally, although multiple scattering is a concern in turbid samples,[43] it is not a concern that is intrinsic to the flow-through SLS apparatus described here. If necessary in other applications, higher-transmission samples may be obtained by using lower refractive index contrast colloidal particles or by reducing the column diameter.

The instrument described here has a number of limitations that should be considered during experimental design. First, as described above, the angular range over which scattering intensity can be measured is limited by the dynamic range of the photodetector and by reflection from the glass flow cell. Additional angular range would be possible by mounting the fiber optic portal to the photodetector on a longer arm (to record scattering at smaller angles) or by applying an antireflective coating to the glass flow cell (to record scattering at angles beyond $\theta = 90°$).

Second, the use of RIM porous media proves to be one of the more difficult challenges for this research. Nafion is chosen for our experiments due to its manageable environmental, safety, and health concerns; its ability to retain colloids; its relative rigidity which ensures that background scattering from the Nafion-fluid interface is constant during each deposition experiment and therefore can be corrected by blank subtraction; and because it allows manipulation of colloidstability by changing the salt concentration. However, Nafion's variable swelling as a function of salt concentration is a drawback. Even small changes in salt concentration (as low as ±1 mM) cause significant changes in grain size, which in turn affects porosity and index matching. These effects become very pronounced at ionic strengths below 25 mM of MgCl$_2$. To avoid excessive variability in Nafion porosity, experiments should either be conducted in deionized water, or alternately with the ionic strength above 25 mM of MgCl$_2$, at which Nafion porosity becomes only marginally dependent on ionic strength.

Third, although fractal dimension and radius of gyration provide real time, spatially distributed, and heretofore inaccessible structural information about colloid deposits in porous media at scales smaller than those accessible by other experimental techniques, they do not provide a unique description of colloid deposit morphology. That is, two deposits with identical mass (i.e., specific deposit), fractal dimension, and radius of gyration could—in principle—have distinct structures reflecting, for example, differences in location with respect to pore throats.[4] This should not be surprising when one considers that, although SLS reflects colloid structure at nanometer-to-micrometer scales, it cannot overcome all the resolution limitations of the optical and microtomography techniques described previously. Accordingly, results gleaned from the instrument described here should be considered as lines of evidence within a broader perspective recognizing the complexity of colloidal phenomena in porous media.

V. CONCLUSIONS

This paper has described a flow-through SLS apparatus that, in conjunction with RIM porous media,provides high resolution, real time, spatially distributed measurement of colloid deposit morphology within porous

media. Granular Nafion in a mixture of isopropanol and water can provide an optically transparent, refractive index matched porous medium. In particular, this instrument makes possible real-time measurement of colloid deposit morphology, which can then be correlated with the corresponding loss of permeability.

ACKNOWLEDGMENTS

REFERENCES

1. A. Alem, N. D. Ahfir, A. Elkawafi, and H. Q. Wang, Transp. Porous Media **106**(2), 303–321 (2015). https://doi.org/10.1007/s11242-014-0402-8
2. R. Armstrong and J. Ajo-Franklin, Geophys. Res. Lett. **38**, L08406, doi:10.1029/2011GL046916 (2011). https://doi.org/10.1029/2011GL046916
3. C. Chen, B. Lau, J. F. Gaillard, and A. I. Packman, Water Resour. Res. **45**, W06416, doi:10.1029/2008wr007252 (2009). https://doi.org/10.1029/2008wr007252,
4. D. C. Mays, J. Environ. Eng. **136**(5), 475–480 (2010). https://doi.org/10.1061/(ASCE)EE.1943-7870.0000173
5. M. Menon, Q. Yuan, X. Jia, A. J. Dougill, S. R. Hoon, A. D. Thomas, and R. A. Williams, J. Hydrol. **397**(1-2), 47–54 (2011). https://doi.org/10.1016/j.jhydrol.2010.11.021
6. J. R. Valdes and J. C. Santamarina, SPE J. **11**(2), 193–198 (2006). https://doi.org/10.2118/88819-PA
7. J. Zhou, X. L. Zheng, M. Flury, and G. Q. Lin, J. Hydrol. **376**(3-4), 557–566 (2009). https://doi.org/10.1016/j.jhydrol.2009.07.067
8. C. J. Werth, C. Y. Zhang, M. L. Brusseau, M. Oostrom, and T. Baumann, J. Contam. Hydrol. **113**(1-4), 1–24 (2010). https://doi.org/10.1016/j.jconhyd.2010.01.001
9. K. Miyahara, Y. Adachi, and K. Nakaishi, Colloids Surf., A **131**(1-3), 69–75 (1998). https://doi.org/10.1016/S0927-7757(96)03961-1
10. K. H. Williams, A. Kemna, M. J. Wilkins, J. Druhan, E. Arntzen, A. L. N'Guessan, P. E. Long, S. S. Hubbard, and J. F. Banfield, Environ. Sci. Technol. **43**(17), 6717–6723 (2009). https://doi.org/10.1021/es900855j
11. A. Kaestner, E. Lehmann, and M. Stampanoni, Adv. Water Resour. **31**(9), 1174–1187 (2008). https://doi.org/10.1016/j.advwatres.2008.01.022
12. N. Ochiai, E. L. Kraft, and J. S. Selker, Water Resour. Res. **42**(12), W12S06, doi:10.1029/2006wr004961 (2006). https://doi.org/10.1029/2006wr004961
13. C. Selomulya, T. M. Tran, X. Jia, and R. A. Williams, AIChE J. **52**(10), 3394–3400 (2006). https://doi.org/10.1002/aic.10967
14. M. R. Wiesner, J. Environ. Eng. **125**(12), 1124–1132 (1999). https://doi.org/10.1061/(ASCE)0733-9372(1999)125:12(1124)
15. D. W. Schaefer, J. E. Martin, P. Wiltzius, and D. S. Cannell, Phys. Rev. Lett. **52**(26), 2371–2374 (1984). https://doi.org/10.1103/PhysRevLett.52.2371
16. G. Bryant, S. Martin, A. Budi, and W. van Megen, Langmuir **19**(3), 616–621 (2003). https://doi.org/10.1021/la026636g
17. G. C. Bushell, Y. D. Yan, D. Woodfield, J. Raper, and R. Amal, Adv. Colloid Interface Sci. **95**(1), 1–50 (2002). https://doi.org/10.1016/S0001-8686(00)00078-6

18. J. Cai, N. Lu, and C. M. Sorensen, Langmuir **9**(11), 2861–2867 (1993). https://doi.org/10.1021/la00035a023

19. A. Heymann, C. Sinn, and T. Palberg, Phys. Rev. E **62**(1), 813–820(2000). https://doi.org/10.1103/PhysRevE.62.813

20. C. M. Sorensen, Aerosol Sci. Technol. **35**(2), 648–687 (2001). https://doi.org/10.1080/02786820117868

21. D. C. Mays, O. T. Cannon, A. W. Kanold, K. J. Harris, T. C. Lei, and B. Gilbert, J. Colloid Interface Sci. **363**, 418–424 (2011). https://doi.org/10.1016/j.jcis.2011.06.046

22. B. Mandelbrot, The Fractal Geometry of Nature (W.H. Freeman and Company, New York, 1982).

23. T. Wakamatsu, Rev. Sci. Instrum. **86**(1), 015112 (2015). https://doi.org/10.1063/1.4906328b

24. M. E. Mont-Eton, M.S. thesis, Department of Civil Engineering, University of Colorado Denver, 2011.

25. E. J. Roth, M.S. thesis, Department of Civil Engineering, University of Colorado Denver, 2013.

26. J. A. Dijksman, F. Rietz, K. A. Lorincz, M. van Hecke, and W. Losert, Rev. Sci. Instrum. **83**(1), 011301 (2012). https://doi.org/10.1063/1.3674173

27. Y. A. Hassan and E. E. Dominguez-Ontiveros, Nucl. Eng. Des. **238**(11), 3080–3085 (2008). https://doi.org/10.1016/j.nucengdes.2008.01.027

28. M. Stöhr, K. Roth, and B. Jähne, Exp. Fluids **35**(2), 159–166 (2003). https://doi.org/10.1007/s00348-003-0641-x

29. M. Elimelech, J. Gregory, X. Jia, and R. A. Williams, Particle Deposition and Aggregation (Butterworth-Heinemann, Boston, 1995).

30. F. M. Pang, C. E. Seng, T. T. Teng, and M. H. Ibrahim, J. Mol. Liq. **136**(1-2), 71–78 (2007). https://doi.org/10.1016/j.molliq.2007.01.003

31. J. A. Rice, Mathematical Statistics and Data Analysis, 2 ed. (Duxbury Press, Belmont, CA, 1995), Sec. 4.6.

32. J. Teixeira, J. Appl. Crystallogr. **21**, 781–785 (1988). https://doi.org/10.1107/S0021889888000263

33. B. Efron and R. J. Tibshirani, in An Introduction to the Bootstrap (Springer, Dordrecht, Netherlands, 1993), Chap. 6.

34. M. H. Kutner, C. J. Nachtsheim, J. Neter, and W. Li, in Applied Linear Statistical Models (McGraw-Hill/Irwin, New York, 2005), Chap. 9.

35. E. J. Roth, B. Gilbert, and D. C. Mays, Environ. Sci. Technol. **49**(20), 12263–12270 (2015). https://doi.org/10.1021/acs.est.5b03212

36. T. Phenrat, N. Saleh, K. Sirk, R. D. Tilton, and G. V. Lowry, Environ. Sci. Technol. **41**(1), 284–290 (2007). https://doi.org/10.1021/es061349a

37. H. Wu, J. J. Xie, M. Lattuada, and M. Morbidelli, Langmuir **21**(8), 3291–3295 (2005). https://doi.org/10.1021/la047403n

38. J. Yon, F. S. Liu, A. Bescond, C. Caumont-Prim, C. Roze, F. X. Ouf, and A. Coppalle, J. Quant. Spectrosc. Radiat. Transfer **133**, 374–381 (2014). https://doi.org/10.1016/j.jqsrt.2013.08.022

39. M. Carpineti, F. Ferri, M. Giglio, E. Paganini, and U. Perini, Phys. Rev. A **42**(12), 7347–7354 (1990). https://doi.org/10.1103/PhysRevA.42.7347

40. Z. Chen, P. Sheng, D. A. Weitz, H. M. Lindsay, M. Y. Lin, and P. Meakin, Phys. Rev. B **37**(10), 5232–5235 (1988). https://doi.org/10.1103/PhysRevB.37.5232

41. M. Lattuada, H. Wu, and M. Morbidelli, Phys. Rev. E **6406**(6), 061404 (2001). https://doi.org/10.1103/PhysRevE.64.061404, , **Google ScholarCrossref**

42. H. Wiese and D. Horn, J. Chem. Phys. **94**(10), 6429–6443 (1991). https://doi.org/10.1063/1.460272

43. I. D. Block and F. Scheffold, Rev. Sci. Instrum. **81**(12), 123107 (2010). https://doi.org/10.1063/1.3518961

44. M. Wozniak, F. R. A. Onofri, S. Barbosa, J. Yon, and J. Mroczka, J. Aerosol Sci. **47**, 12–26 (2012). https://doi.org/10.1016/j.jaerosci.2011.12.008

45. J. S. Pedersen, Adv. Colloid Interface Sci. **70**, 171–210 (1997). https://doi.org/10.1016/S0001-8686(97)00312-6